

# Bistable behavior of a Kerr lens mode locked Ti:Sapphire laser

Marcelo G. Kovalsky<sup>1</sup> and Alejandro A. Hnilo<sup>2</sup>

Centro de Investigaciones en Láseres y Aplicaciones (CEILAP- CONICET). Instituto de Investigaciones Científicas y Técnicas de las Fuerzas Armadas (CITEFA). San Juan Bautista de La Salle 4397, Villa Martelli, Buenos Aires, Argentina

1 Investigador Asistente, CONICET

2 Investigador Independiente, CONICET

## Abstract

Kerr lens mode locked Ti:Sapphire lasers can operate in at least two pulsed modes. Several models were developed with the aim to describe the characteristics of these modes. Those based on iterative maps, can reproduce the structurally stable properties of each mode but are unable to describe the interaction between modes. In this paper, we present a numerical simulation based on a complete map equation that makes possible to accurately describe the bistability experimentally observed in the laser. With the numerical time series we determine that the bistable behavior corresponds to low dimensional deterministic chaos and calculate that the embedding dimension of the attractor is three.

## 1. Introduction

The phenomenon of optical bistability, in which certain parameters of a nonlinear system have two stable states, was first reported by Gibbs *et al.* in 1976.[1] Since then a large number of studies on optical bistability have been published (see, for example, the review in Ref. 2). The prior research includes bistability in a CO<sub>2</sub> laser with an intracavity saturable absorber [3] and systems with temperature-induced bistability, where the absorption coefficient or the index of refraction is temperature dependent.[4–6]. In Ti:Sapphire lasers bistability between pulsed modes of operation has been theoretically predicted and experimentally observed [7].

Beyond of its many application in almost any field of science and technology, the KLM Ti:Sapphire laser is, by itself, a very intricate dynamical system. This complexity arises primarily because of the nonlinear interlacing among the pulse variables that appears in the Kerr medium. There are two main nonlinear factors. One of them is the formation of an intensity-dependent lens. The other factor is an intensity-dependent frequency sweep (or chirp), known as self-phase modulation (SPM).

A standard approach to a complex nonlinear system reduces the study of the continuous time dynamics to the study of an associated discrete time system, the iterative, stroboscopic or Poincaré map [8]. A map is a sequence of values of the variables taken at discrete times. The description with maps is an alternative to that with a differential equation, and no information is gained or lost. There are, however, some immediate advantages: the dimensionality of the problem is reduced in (at least) one and the numerical simulations are easier and faster. However, most of the times, writing the map equation can be as difficult as solving the partial differential equation, unless the physical system has some “internal clock” that determines the position of the adequate discrete times. In the case of passive mode-locked lasers, that clock is provided by the cavity round trip time and, in fact, it is easy to obtain recursive equations linking the pulse variables in the (n-1) round trip with the values taken at the n-round trip [9]. The stability of periodical solutions (as the mode-locking pulse train) is determined easily. There are additional advantages when studying unstable behaviors: there is no theoretical limitation on the acceptable pulse variation from one round trip to the next, and the observed period doubled solutions [10-12] are trivially described with maps. However, in order to obtain semi analytical expressions of the pulse variables it is necessary to make some assumptions about the strength of the nonlinearities [13]. The main consequence of this approach is that we lose the ability to simultaneously describe the several pulsed modes of operation of the laser. In this paper, on the contrary, we make no assumptions on the nonlinearities. As a result we can reproduce the bistable behavior between transform limited pulses and chirped pulses observed experimentally as well as accurately describe, through numerical simulation with the complete map and time series analysis, the characteristics of the attractor of this kind of bistability.

## 2 Map model

We start by supposing that the electric field inside the mode-locking pulse, as a function of the distance to the optical axis  $r$  and the time  $t$ , is given by:

$$E(t) = E_0 \exp(-i kr^2/2q) \exp(-i kt^2/2p) \quad (1)$$

where  $p$ ,  $q$ :

$$\frac{1}{p} = Q - i \frac{n \lambda}{\pi \tau^2} \quad (2)$$

$$\frac{1}{q} = \frac{n}{R} - i \frac{n \lambda}{\pi \sigma^2} \quad (3)$$

are functions of the pulse variables: the spot radius  $\sigma$ , the beam curvature radius  $R$ , the pulse duration  $\tau$  and the chirp  $Q$  (this is the second derivative of the phase with respect to the time). There is a fifth pulse variable, the energy  $U$ . As the pulse propagates through an optical element or distance, the  $p$  and  $q$  parameters change according to:

$$q_{\text{out}} = (A \cdot q_{\text{in}} + B) / (C \cdot q_{\text{in}} + D) \quad (4)$$

where  $\{A \dots D\}$  are the elements of a  $2 \times 2$  matrix. The same holds for  $p$  [14,15]. The matrix describing the whole laser cavity is obtained by multiplying the matrix describing each optical component. In general, the propagation is fully described by  $4 \times 4$  matrices. In this way, it is easy to obtain the matrix that describes the effect of a round trip inside the laser cavity (Fig. 1). In the case of Ti:sapphire lasers, the Gaussian approximation (1) is valid for pulses longer than 10 fs [15], and, under appropriate design conditions [14] (which usually hold for Ti:sapphire laser cavities) the general  $4 \times 4$  round trip matrix can be split into two diagonal blocks of  $2 \times 2$ . Therefore, the effect of a round trip on the parameters  $p, q$  can be described with a matrix of the form:

$$M = \begin{pmatrix} A & B & 0 & 0 \\ C & D & 0 & 0 \\ 0 & 0 & K & I \\ 0 & 0 & J & L \end{pmatrix} \quad (5)$$

The nonlinearity arises from the fact that the matrix elements include terms (due to the self-focusing and SPM in the laser rod) which are functions of the pulse variables. These terms, named here nonlinearities have the general form:

$$\gamma = c_{\gamma} \frac{U}{\tau \sigma^4} \quad (6)$$

for the matrix elements ABCD and:

$$\beta = c_\beta \frac{U}{\sigma^2 \tau^3} \quad (7)$$

for the matrix elements KIJL. The constants  $c_\gamma$ ,  $c_\beta$  are proportional to the nonlinear index of refraction of the Ti:sapphire. The complete expression of the nonlinearities as functions of the pulse's parameters is not trivial [16]. Its distinctive feature is that the nonlinearity is assumed to be effective over the Rayleigh length, rather than the entire Ti:Sapphire rod's length, and that the value of the Rayleigh's length is calculated for the continuous wave (zero nonlinearity) case. It is convenient to define new variables:  $S = \sigma^{-2}$ ;  $T = \tau^{-2}$ ;  $R = \rho^{-1}$ . The expressions that link the variable values at the (n -1)-round trip with the ones at the n-round trip are then:

$$S_{n+1} = \frac{S_n}{(\mathbf{A} + \mathbf{B}\rho_n)^2 + (\mathbf{B}\lambda S_n)^2} \quad (8)$$

$$\rho_{n+1} = \frac{(\mathbf{A} + \mathbf{B}\rho_n)(\mathbf{C} + \mathbf{D}\rho_n) + \mathbf{B}\mathbf{D}(\lambda S_n)^2}{(\mathbf{A} + \mathbf{B}\rho_n)^2 + (\mathbf{B}\lambda S_n)^2} \quad (9)$$

$$T_{n+1} = \frac{T_n}{(\mathbf{K} + \mathbf{I}Q_n)^2 + \left(\frac{\mathbf{I}T_n}{\pi}\right)^2} = T_n \frac{\mathbf{L} - \mathbf{I}Q_{n+1}}{\mathbf{K} + \mathbf{I}Q_n} \quad (10)$$

$$Q_{n+1} = \frac{(\mathbf{K} + \mathbf{I}Q_n)(\mathbf{J} + \mathbf{L}Q_n) + \mathbf{I}\mathbf{L}\left(\frac{T_n}{\pi}\right)^2}{(\mathbf{K} + \mathbf{I}Q_n)^2 + \left(\frac{\mathbf{I}T_n}{\pi}\right)^2} \quad (11)$$

The equation for the energy U is found by expansion of the usual equation of gain saturation

for the mean values  $S^*$  and  $U^*$

$$U_{n+1} = U_n \left\{ 1 - \frac{2}{\mu} \left( \frac{U^* S_n + U_n S^*}{D_s} \right) + 4 \frac{\mu-1}{\mu} \right\} \quad (12)$$

where  $\mu$  is the product of the small signal gain and the single passage feedback factor due to linear or passive losses (mirror's reflectivities, scattering, etc.), and  $D_s \approx 1.2 \text{ mJ / cm}^{-2}$  is the saturation energy flux (i.e., the saturation energy multiplied by the cavity round trip) for Ti:sapphire.

The matrix elements in Eqs. (8)-(11) include the nonlinearities. It is convenient to express them as a series expansion:

$$\mathbf{A} = \mathbf{A}_0 + \gamma \mathbf{A}_\gamma + \gamma' \mathbf{A}'_\gamma + \gamma^2 \mathbf{A}^{(2)}_\gamma + \gamma'^2 \mathbf{A}'^{(2)}_\gamma + \gamma\gamma' \mathbf{A}''^{(2)}_\gamma + \dots \quad (13)$$

the same for B, C, D, and:

$$\mathbf{K} = 1 + 2\delta\beta' \quad (14)$$

$$\mathbf{I} = 2\delta \quad (15)$$

$$\mathbf{J} = 2\delta\beta\beta' + \beta + \beta' \quad (16)$$

$$\mathbf{L} = 1 + 2\delta\beta \quad (17)$$

where  $2\delta$  is the value (negative) of the group velocity dispersion (GVD) per round trip, We employ the net GVD inside the cavity as the main control parameter. The coefficients of the expansions (13) are functions of the geometrical parameters only. The factors  $\gamma$  and  $\beta$  are the nonlinearities, as defined by Eqs. (5) and (6), when the pulse crosses the rod from M3 to M2 (i.e., towards the output mirror). The factors  $\gamma'$  and  $\beta'$  are the nonlinearities when the pulse crosses the rod from M2 to M3. The recursive relations (8)-(11) and (14)-(17) are the iterative map describing the laser dynamics. The fixed points of the map of the laser are obtained by imposing that the variables at the (n -1)-round trip are equal to the ones at the n-round trip. The  $\{\mathbf{A} \dots \mathbf{L}\}$  elements include the nonlinearities which, in turn, are functions of the pulse

variables. The general problem is intractable analytically. It can be solved in a closed form by assuming that only the first order in the nonlinearities is relevant. This is a good approximation for pulses longer than 10 fs, a limit we are anyway restricted because of the Gaussian pulse approximation (1).

### 3 Bistability between laser modes

The KLM Ti:Sapphire laser is experimentally known to display three modes of operation: continuous wave (named  $P_0$ ), mode locking of transform limited pulses (named  $P_1$ ) and mode locking of (positive) chirped pulses (named  $P_2$ ). These three modes of operation correspond to three fixed points of the map equation. A fourth mode, named  $P_3$ , (negative chirped pulse) is predicted from the map equation but not observed in the real laser. In the figure 2 we plot the calculated regions of stability of the three predicted mode locked solutions as a function of two parameters: the position of the output mirror ( $x$ ) and the net intracavity GVD.

One of the main advantages of the maps approach is that the stability of the solutions against perturbations can be easily computed, by solving the eigenvalue equation of the linearized map evaluated at the fixed point. Where the moduli of one or more eigenvalues becomes larger than 1, the corresponding fixed point becomes unstable.

From the stability regions plot one can see the coexistence of the three modes, as well as the bistability between  $P_1$  and  $P_2$  and  $P_2$  and  $P_3$ . Also the graphics shows a broad area of bistability and even multistability in the phase space. However the experimental evidence as well the map model presented in this paper show no multistability nor bistability between  $P_2$  and  $P_3$ . The reason lies in the numerical magnitude of the eigenvalues of each pulsed mode. In figure 3 the eigenvalue's modulus is depicted as a function of the net intracavity GVD for the three pulsed modes. The moduli of the eigenvalues are a measure of the actual ability of the fixed point to retain the system. In this way the system is never attracted to  $P_3$  because the eigenvalues moduli of  $P_3$  are very close to 1 and always remain larger than those of  $P_1$  and  $P_2$  and only the bistability between  $P_1$  and  $P_2$  is possible.

We use the complete map in order to determine the actual extension of the bistable region. For a given laser geometry, we scan the net intracavity GVD and determine that the system displays bistability from  $-39\text{fs}^2$  to  $-46\text{fs}^2$ . On the other hand, for a fixed value of GVD, in our simulation  $-42\text{fs}^2$ , the bistable region using the distance  $M_1 - M_2$  as a parameter, is 3 centimeters wide, that is the distance  $M_1 - M_2$  can be modified between 57.4cm and 60.4cm.

We run the map equations (8)-(11) with initial values for the pulse variables close to the fixed point  $P_2$  and a value of net intracavity GVD of  $-42\text{fs}^2$ . The figure 4 displays the simulated time

series of the pulse duration. Bistable behavior is revealed immediately. It is clear that the pulse duration switches spontaneously between two well defined regions and roughly, the pulse duration of  $P_2$  is twice the duration of  $P_1$ , as it is predicted by the map model of the reference [7]. Another remarkable improvement that introduces this map is the accurate measurement of the wide (in the control parameter  $\delta$ ) of the full transition from stable mode locked pulses to full developed chaos. As the map model of reference [7] is unable to take into account the interaction between modes, the region of transition from stable mode locking to full developed chaos predicted by that model is much larger than the actual one. The complete map equation of this paper overcomes this problem and predicts a whole transition width of  $39\text{fs}^2$  in excellent agreement with the  $40\text{fs}^2$  measured in the experiment [17].

#### 4 Description of the attractor

As a first approximation to the behavior of the attractor we study the statistics of the bistable time series. From the histogram (figure 5) it is clear that two different regimes are present. We also see that the number of occurrences of each mode are quite distinct. In the bistable region,  $P_1$  appears more often than  $P_2$  with a variable ratio that depends of the GVD parameter. It is noteworthy, as we can see in table 1, how the number of  $P_2$  hits diminishes as we change the net intracavity GVD, that is as we move to the region where the  $P_2$  is more unstable and  $P_1$  is still stable. Of course, once we reach the limit value of GVD for the bistable operation only  $P_1$  is present.

To give an insight into the way bistability actually works, we start with the reconstruction of a pseudo phase space from the one dimensional time series of the physical variables of the laser. This procedure gives the same result that the delay – coordinate technique as guarantees the embedding theorem [18]. We then use a combination of Grassberger – Procaccia (GPA) analysis and false nearest neighbors (FNN) analysis to obtain the correlation and embedding dimensions for the data. These two analyses distinguish clearly between random noise (which is high dimensional) and low- dimensional, deterministic chaos. In the GPA the correlation dimension  $D_2$  is calculated as a function of the embedding dimension  $E$ . It is expected that, for white noise  $D_2$  increases linearly with unity slope. In our case  $D_2$  clearly converges, indicating that the data are not generated by noise. As a further confirmation we calculate the Lyapunov exponents finding that as we decrease the net GVD - that is, as we move into the unstable zone - in all the cases there is one positive Lyapunov exponent ( see table 2). In this way we confirm that data are indeed generated by a nonlinear, low dimensional, deterministic chaos. The embedding dimension of the attractor can be estimated using the FNN technique, in which the number of neighbors in an  $E$ -dimensional reconstructed phase space is compared with that in

$E+1$  dimensions. For low dimensional, deterministic chaos, the number of false neighbors should fall to zero at a relatively small value of  $E$ . For high dimensional chaos and for random signal, on the contrary, the FNN will level off at a nonzero value, and may even rise again as  $E$  is increased. As we can see in the figure 6 the FNN analysis of our chaotic data set in the bistable region between  $P_1$  and  $P_2$  gives an embedding dimension of three.

The figure 7 shows the correlation dimension of the attractor in the bistable region. From the graphics we can estimate that  $D_2$  dimension has a value between 1 and 2. As the embedding dimension is three it is possible to plot the attractor in phase space. The shape of the attractor can be seen in the figure 8 where the bistable nature is once again revealed .

## **Summary**

In conclusion we develop a map model that is capable to explain not only the pulsed mode locked modes of operation of a Kerr lens mode locked Ti: Sapphire laser, but also describes accurately the bistable behavior observed in the experiments. With the help of the simulated time series we determine that the bistability between transform limited pulses and chirped pulses responds to low dimensional deterministic chaos. In particular the attractor of the system is a strange attractor because we measure a non integer  $D_2$  dimension and the embedding dimension is three which makes possible to plot the whole attractor in the phase space.

## **Acknowledgements**

This work was supported by the contracts PICT 14240 BID 1728 OC-AR of the Agencia Nacional de Promoción Científica y Tecnológica (ANPCyT) .

## References

- [1] H. M. Gibbs, S. L. McCall, and T. N. C. Venkatesan, “Differential gain and bistability using a sodium-filled fabry–perot interferometer,” *Phys. Rev. Lett.* **36**, 1135–1138 (1976).
- [2] A. E. Siegman, “Bistable optical systems,” in *Lasers* (University Science, Mill Valley, Calif., 1986), Chap. 13.7.
- [3] E. Arimondo and B. M. Dinelli, “Optical bistability of a CO<sub>2</sub> laser with intracavity saturable absorber: experiment and mode,” *Opt. Commun.* **44**, 277–282 (1983).
- [4] Janossy, M. R. Taghizadeh, J. G. H. Mathew, and S. D. Smith, “Thermally induced optical bistability in thin film devices,” *IEEE J. Quantum Electron.* **QE-21**, 1447–1452 (1985).
- [5] L. Kowalczyk, B. Koziarska-Glinka, L. V. Khoi, R. R. Galazka, and A. Suchocki, “Near band-gap optical nonlinearities and bistability in Cd<sub>12x</sub>MnxTe,” *Opt. Mater.* **14**, 161–170 (2000).
- [6] D. R. Gamelin, S. R. Luthi, and H. U. Gudel, “The role of laser heating in the intrinsic optical bistability of Yb<sup>3+</sup>-doped bromide lattices,” *J. Phys. Chem.* **104**, 11045–11057 (2000).
- [7] M.G. Kovalsky , A.A. Hnilo, A.R. Libertun and M.C. Marconi “Bistability in Kerr lens mode locked lasers” *Opt. Commun.* **192**, 333-338 (2001).
- [8] S. Wiggins, “Introduction to applied nonlinear and dynamical systems and chaos”, Springer, New York, 1990.
- [9] A.A. Hnilo, ‘Self mode locking Ti:Sapphire laser description with an iterative map’ *J. Opt. Soc. B* **12** 4 (1995).
- [10] D. Cote, H. van Driel, “ Period doubling of a femtosecond Ti:Sapphire laser by total mode locking” *Opt. Lett.* **23** 715 (1998) .
- [11] G. Sucha, S. Bolton, S. Weiss, D. Chemla, “ Period doubling and quasi-periodicity in additive- pulse mode – locked lasers” *Opt. Lett.* **20** 1794 (1995).
- [12] M.G. Kovalsky, A.A. Hnilo and C.M.F.G. Inchauspe, “ Hidden instabilities in the Ti:Sapphire Kerr lens mode locked laser” *Opt.Lett.* **24** 1638 (1999).
- [13] M.G. Kovalsky and A.A. Hnilo, “Stability and bifurcation in Kerr lens mode locked Ti:Sapphire lasers” *Opt. Commun.* **186**, 155 -166 (2000).
- [14] A. G. Kostenbauder “Ray pulse matrices: a rational treatment for dispersive optical systems” *IEEE J. Quantum Electron.* **26**, 1148 (1990).
- [15] O E Martinez and J Chilla “Self mode locking of Ti”Sapphire lasers: a matrix formalism” *Opt. Lett.* **17**, 1210 (1992).
- [16] M. Marioni and A. Hnilo “ Self starting of self mode locking Ti:Sapphire lasers. Description with a Poincare map” *Opt. Commun.* **147**, 89 (1998).
- [17] M. Kovalsky and A. Hnilo “ Different routes to chaos in the Ti:Sapphire laser” *Phys. Rev. A*, **70**, 043813 (2004).

[18] H.D.I.Abarbanel, "Analysis of observed chaotic data" Springer – Verlag, New York (1996).

Figures

Figure 1

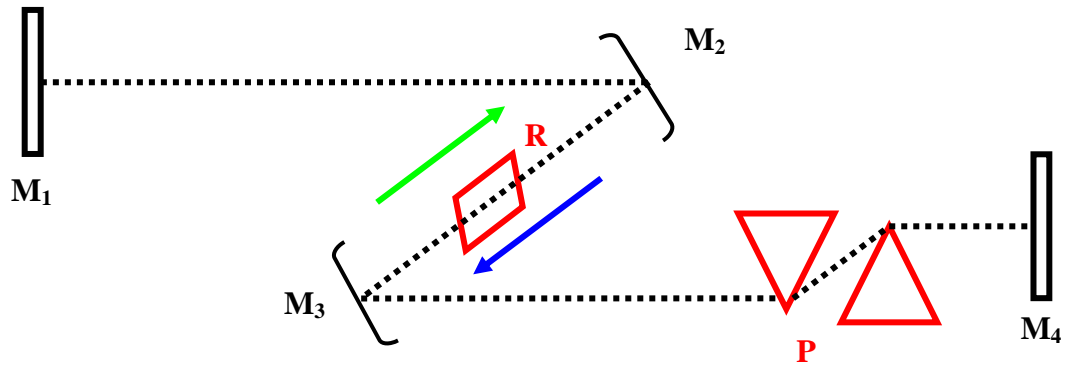


**Figure 2**

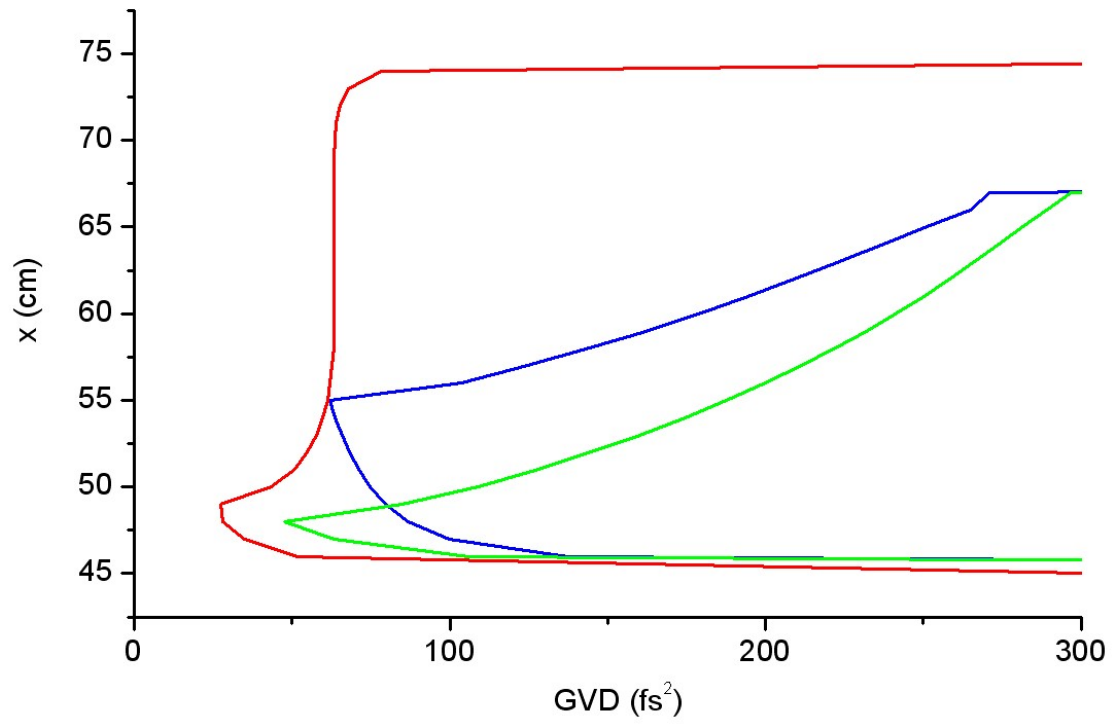


**Figure 3**

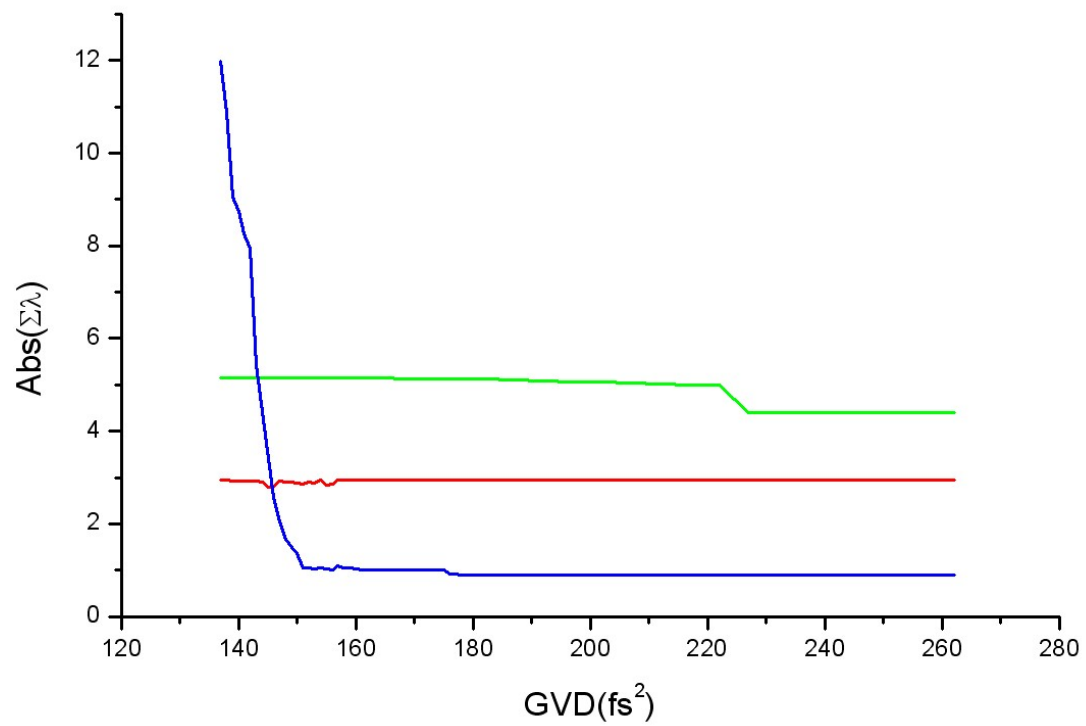


**Figure 4**

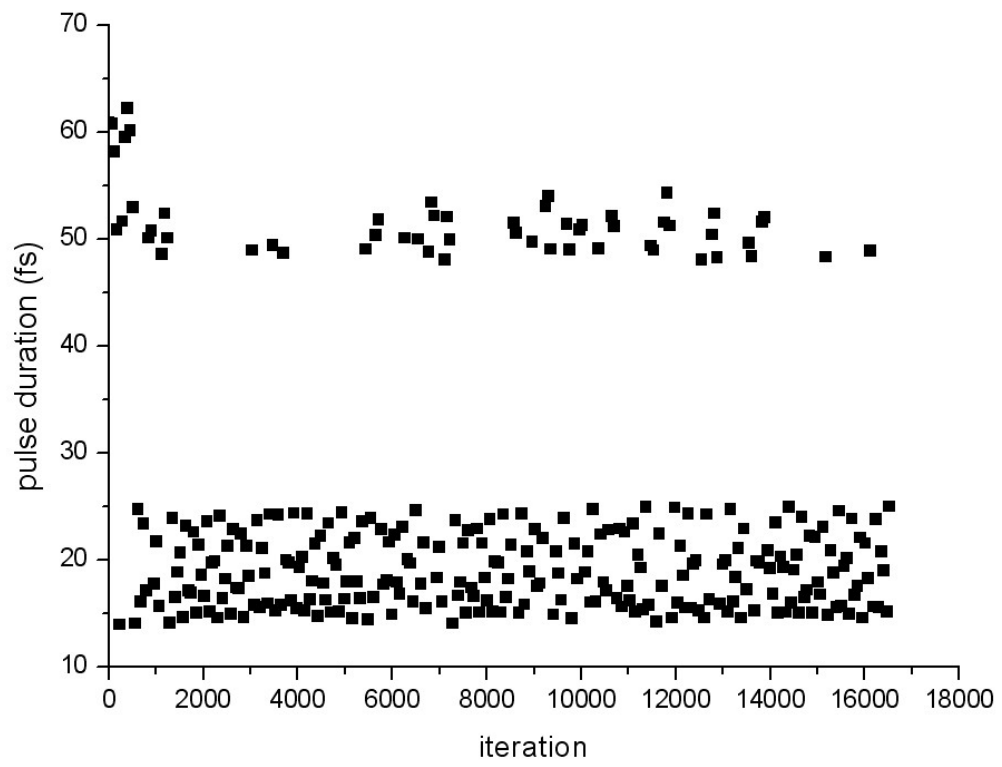


**Figure 5**

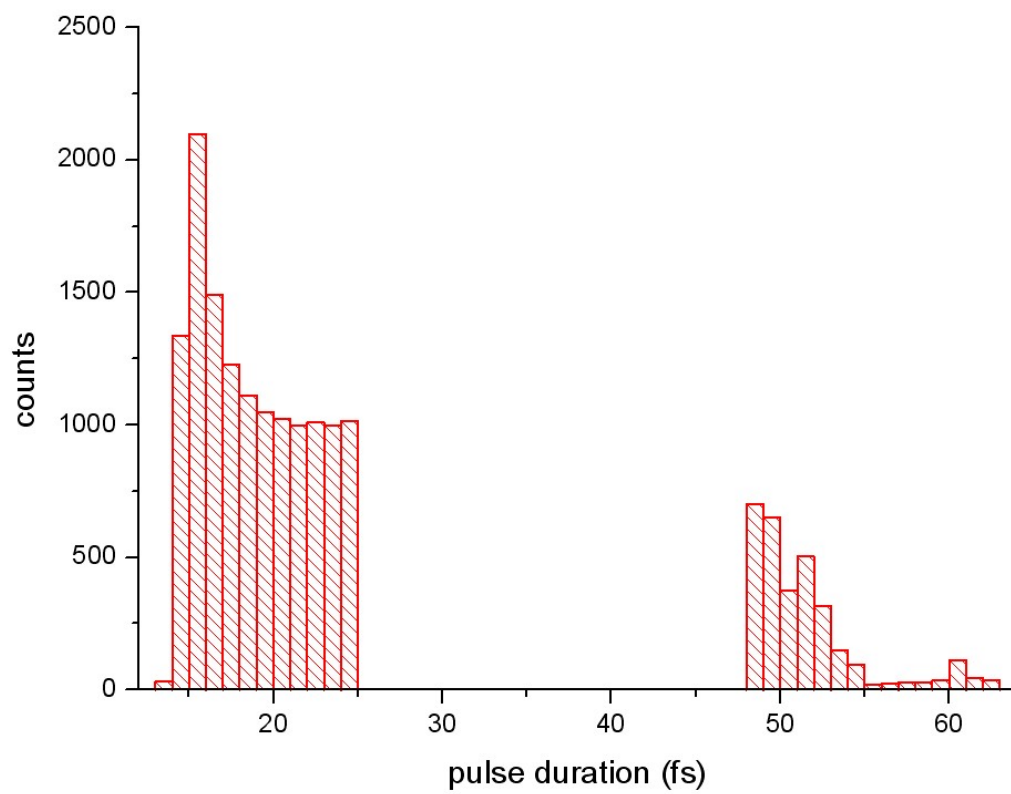


**Figure 6**

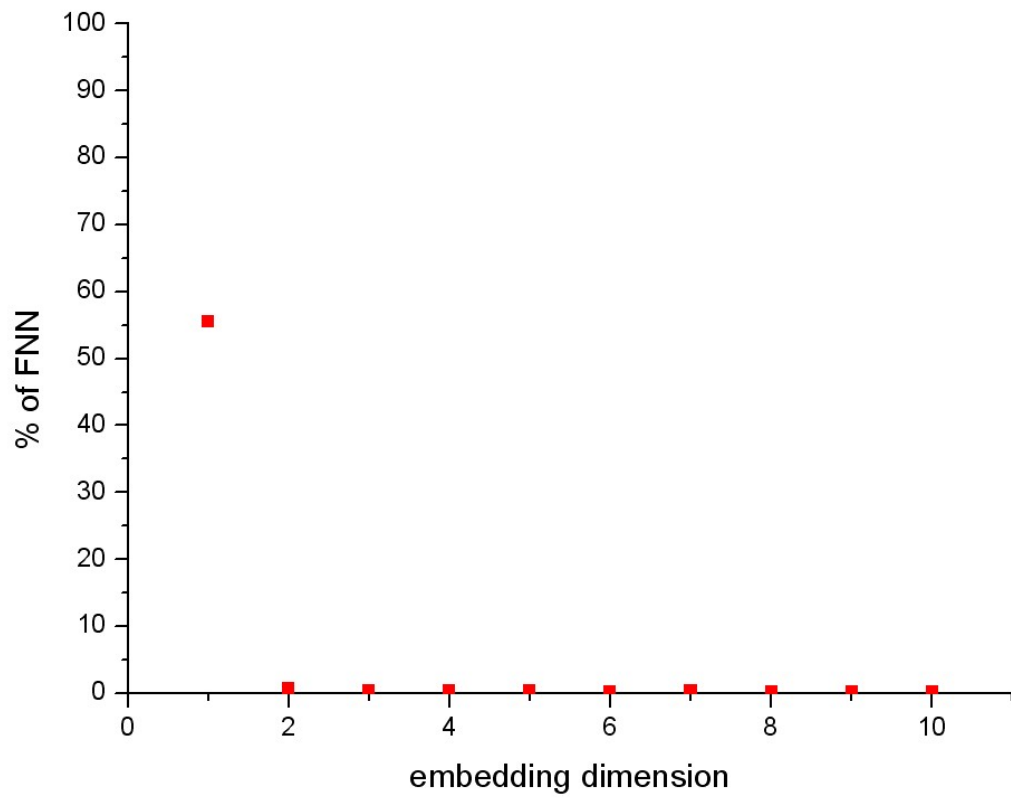


**Figure7**

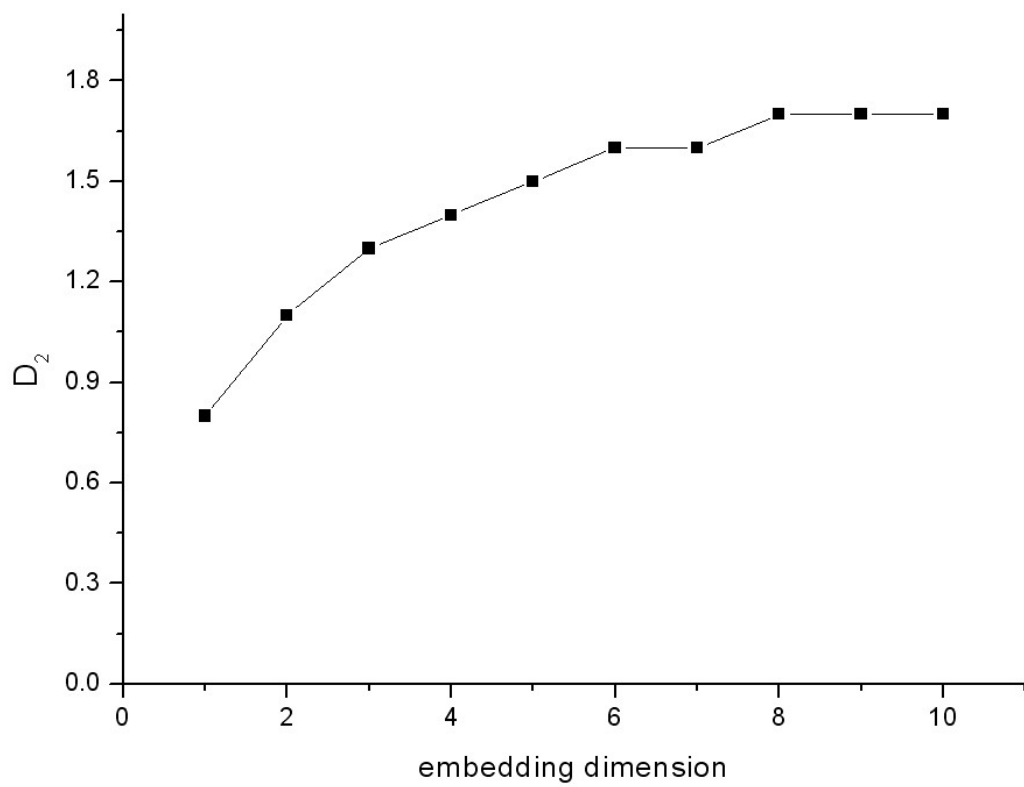
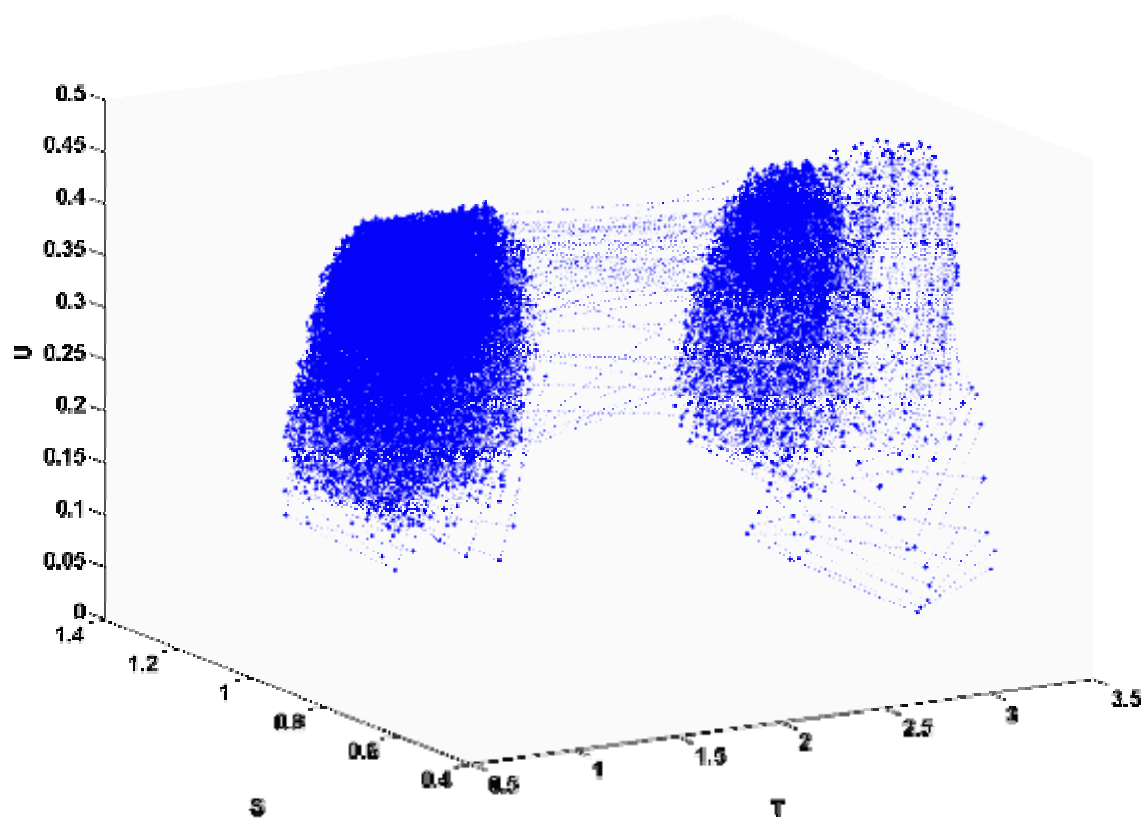


Figure 8



## Tables

**Table 1**

$\delta$	C
<b>-40</b>	<b>0.285</b>
<b>-41</b>	<b>0.213</b>
<b>-42</b>	<b>0.203</b>
<b>-43</b>	<b>0.039</b>

**Table 2**

$\delta$	$\lambda_1$	$\lambda_2$	$\lambda_3$
-40	0.03743	-0.03943	-0.88609
-41	0.05683	-0.09577	-1.21351
-42	0.07663	-0.16451	-1.18888
-43	0.02804	-0.23133	-1.09102

## Figure Captions

**Figure 1:** Scheme of the laser cavity.  $M_1$ : exit mirror;  $M_2, M_3$ : focusing mirrors; R: Ti:Sapphire rod; P: pair of prisms for GVD compensation;  $M_4$ : end mirror. The arrows indicates the direction of the nonlinearities in the map equation, blue: primed nonlinearities, green: non primed nonlinearities.

**Figure 2 :** Stability regions of the three pulsed modes of operation of the KLM Ti:Sapphire laser. Horizontal axis: negative net intracavity GVD. The lines indicate the border of each stability zone. The confined region is the stable one.

**Figure 3 :** Numerical magnitude of the sum of the eigenvalues in function of the (negative) net intracavity GVD . As the number of variable's system is five, the corresponding fixed point will be stable if the eigenvalue modulus remains under 5.

**Figure 4 :** Time series of the pulse duration variable of the complete map with a value of intracavity GVD of  $-42\text{fs}^2$ . In the horizontal axis we plot the iteration of the map equation that represents a round trip in the laser cavity.

**Figure 5 :** Histogram of a time of the complete map equation. The net GVD value used was  $-43\text{fs}^2$ . Note that the two sets of data shows a completely different statistical distribution, indicating the different behavior of the two pulsed modes.

**Figure 6 :** Graphics of the percentage of the false nearest neighbors as a function of the embedding dimension. From the plot we see that the embedding dimension is three. In dimension two the percentage of FNN is 0.9% and fall to zero in dimension 3.

**Figure 7 :** Fractal dimension,  $D_2$ , as a function of the embedding dimension . The time series employed in this plot was run with a value of net GVD of  $-43\text{fs}^2$  that corresponds to the bistable region. From the graphics the fractal dimension is approximately 1.7.

**Figure 8** : Representation of the whole attractor of the bistable region. In the plot we the physical meaning variables X axis(T): pulse duration normalized to the mean value of the time series; Y axis (S): spot size of the pulse; Z axis (U): energy of the pulse, all variables are normalized to the mean value and hence are adimensional.

**Table 1** : In this table can be seen the evolution of C, the ratio of  $P_2 / P_1$  occurrences in the bistable zone as a function of  $\delta$ , the net intracavity GVD ( in  $\text{fs}^2$ ). Observe the sudden change in C when  $\delta$  is very close to the bistable border.

**Table 2** : Lyapunov exponents ( $\lambda$ , in  $\text{s}^{-1}$ ) of the time series in the bistable zone. Note that in all cases there is one positive exponent, revealing the chaotic nature of the system.